Integration of an Ultra-Short Polarization Rotator on an Active-Passive Indium Phosphide Membrane

Sander Reniers
Photonic Integration
Eindhoven University of Technology
Eindhoven, The Netherlands
s.f.g.reniers@tue.nl

Kevin Williams
Photonic Integration
Eindhoven University of Technology
Eindhoven, The Netherlands
k.a.williams@tue.nl

Jos van der Tol
Photonic Integration
Eindhoven University of Technology
Eindhoven, The Netherlands
j.j.g.m.v.d.tol@tue.nl

Yuqing Jiao
Photonic Integration
Eindhoven University of Technology
Eindhoven, The Netherlands
y.jiao@tue.nl

***Abstract*—We present the technology development for the integration of an ultra-short polarization rotator on an active-passive indium phosphide membrane platform. The technology is proven with two demonstrator circuits: a polarization-independent semiconductor optical amplifier and a dual-polarization light source. Experimental results for both circuits are presented in this paper.**

***Index Terms*—photonic integrated circuit, polarization, semiconductor optical amplifier**

I. Introduction

To keep up with the ever-increasing bandwidth requirement for our data-communication systems, every degree of freedom should be exploited. To satisfy this demand, optical communication systems have earned their place in the last decades, since it offers high bandwidth and efficiency. To fully utilize the bandwidth capabilities of this technology, phase, amplitude and polarization are commonly used in modulation schemes. Photonic integration platforms offer excellent capability to modulate and demodulate signals sent over an optical fiber link with high speed and low power-consumption. Phase and amplitude modulation is often carried out on-chip, where polarization functions are often taken off-chip, using optics. Integrated polarization rotator have been a topic of interest for research for many years on various platforms, e.g. indium phosphide based platforms [1], [2] and silicon photonics [3], [4]. Integration on a full active-passive platform enables on chip polarization multiplexing and advanced modulation schemes utilizing the polarization state, e.g. Stokes-vector modulation [5]–[7]. For these applications, integrated polarization rotators are of paramount importance. In this paper, we present the experimental demonstration of an ultra-short integrated polarization rotator on an indium phosphide (InP) membrane platform. The InP-membrane-on-silicon (IMOS) platform [8] offers high optical confinement through its high index-contrast waveguides. This high index-contrast enables nanophotonic waveguides by adhesive bonding of an InP wafer to a silicon carrier wafer by using benzo-cyclo-butene (BCB) as an adhesive. A typical passive waveguide has a width of 400 nm and a height of 300 nm, and guides both the fundamental transverse electric (TE) and transverse magnetic (TM) modes. The polarization rotator [9] on the IMOS platform is created by a unique triangular-shaped structure, which is extremely compact (<5 μm long), and achieves over 97% polarization conversion efficiency [10]. It requires an extra epitaxial layer for fabrication, and hence has only been realized on a dedicated fabrication run so far. In this paper, we present the integration technology for integration of the polarization rotator on the twin-guide active-passive IMOS platform [11]. First, the polarization rotator is introduced. Then, the technology that enables the integration of the rotator is presented in detail. Two experimentally demonstrated circuits are characterized and discussed.

The authors acknowledge the use of NanoLab@TU/e facilities.

II. Polarization rotator

The design of the polarization rotator is shown in Fig. 1. The rotator consists of two triangular sections, with a short rectangular section in between. It utilizes mode hybridization to achieve polarization conversion [9]. The modes in the triangular sections have a tilt angle of 28°, thus two sections are required to achieve full polarization conversion. The triangular sections are created by using a wet etchant that stops on the $\{112\}$ crystal plane of InP [12]. A scanning-electron microscope (SEM) image of a fabricated polarization rotator is shown in Fig. 2. The image is taken before wafer bonding.

III. Integration technology

To integrate the polarization rotator, extra epitaxial layers are required for the top part of the device with respect to the standard twin-guide layer stack. To provide the necessary background, the platform is briefly introduced. On the platform, the active building blocks, such as semiconductor optical

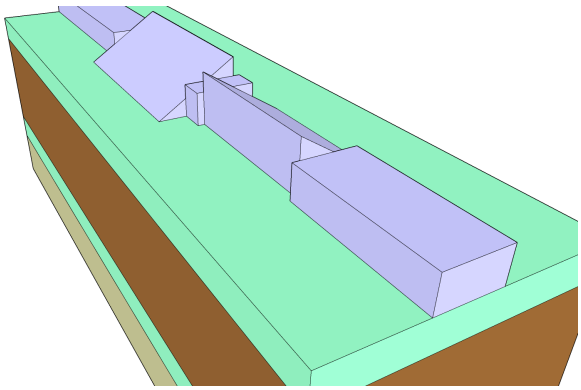

Fig. 1. Schematic of the IMOS polarization converter.

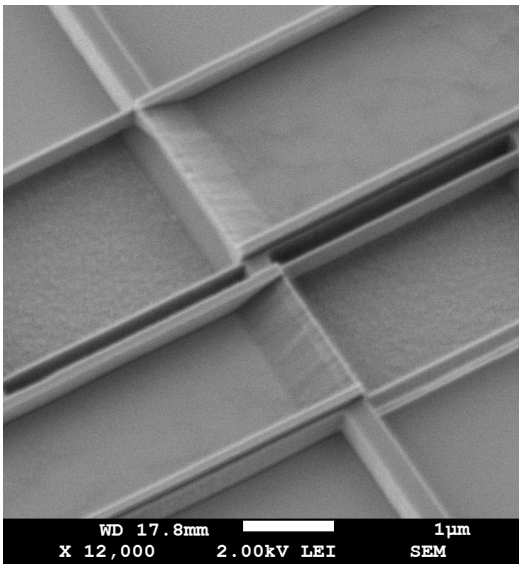

Fig. 2. Scanning electron microscope image of a fabricated polarization converter before bonding.

amplifiers (SOAs), are coupled to the passive waveguides by using adiabatic tapers. Therefore, the active and passive layers are separated, which is depicted in Fig. 3. In this figure, the full layer stack of the platform is shown. The multi-quantum-well (MQW) active core and passive InP waveguide layer can be seen here. To accommodate the polarization rotator, we choose to use the n-doped InP layer for the top of the triangular section. This is chosen over adding extra epitaxial layers on the other side of the passive waveguide, since the n-doped InP is already present and requires minimal change to the existing layer stack. Also, this enables fabrication of the polarization rotators before wafer bonding, which is preferred over processing the rotators after bonding, since this has proven to be safer when doing wet etching. For this reason, the thickness of this layer is chosen such that the height of the triangular section is optimal. Since the height of the section defines the complete geometry of the sections, the optimal height is found by finding the best overlap with a standard waveguide, which is 460 nm. Since the n-doped InP layer is

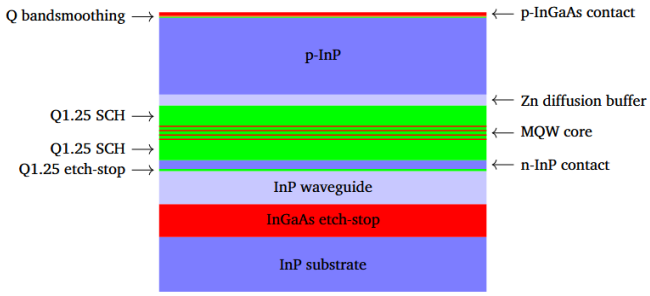

Fig. 3. Twin-guide active-passive layer stack.

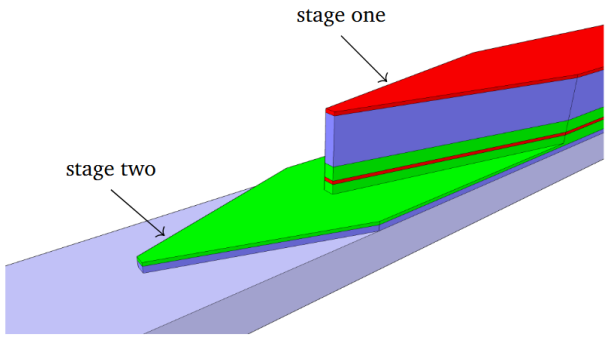

Fig. 4. Schematic of the double stage active-passive taper for the twin-guide IMOS platform.

between the active core and the passive InP waveguide, the twin-guide taper design needs to be reconsidered.

A. Active-passive taper

Since the n-doped InP layer thickness is increased from 80 nm to 140 nm compared to previous fabrication runs, the tapers need to be reconsidered as part of the technology development of the integration. An initial version of the taper is separately presented in [13], the final design is shown schematically in Fig. 4. From a finite-difference time-domain (FDTD) simulation of the taper an insertion loss of 0.4 dB and a back-reflection of -47.5 dB are obtained for a total taper length of 45 µm: 30 µm for stage one and 15 µm for stage two. The fabrication of the tapers is carried out at the same time as the polarization rotators, for which the key steps are presented in the next section.

B. Process-flow for fabrication

The key fabrication steps for the integration are shown in Fig. 5. Since fabrication of the polarization rotators is carried out before the wafer bonding, this is still on an InP substrate. Only the key steps that demonstrate the fabrication of the rotators are shown here.

The first step is to deposit a thick layer of SiN_x (200 nm) with plasma-enhanced chemical vapor deposition (PECVD). This will be used for multiple consecutive lithography steps. The starting stack for the fabrication of the devices is shown in Fig. 6. In the first lithographic step, part of the taper

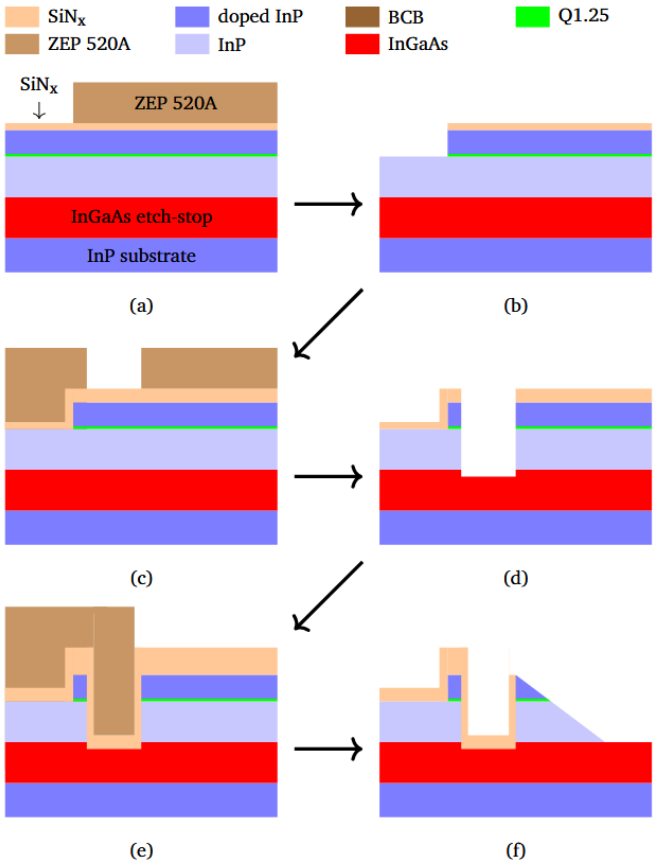

Fig. 5. Overview of key steps of PR fabrication process. (a) Etching of SiN_x mask. (b) Wet etching of n-doped InP and Q1.25 etch-stop layer. (c) New layer of SiN_x deposited and lithography for etching of vertical sidewall of PR sections. (d) Etching of vertical sidewall of PR sections. (e) New layer of SiN_x deposited and lithography for wet etching of sloped sections of PRs. (f) Wet etching of sloped section of PRs.

between the active and passive components is defined. For the polarization rotators all areas will be opened in this lithography, and the Q1.25 (InGaAsP with a band gap of 1.25 µm) separate confinement hetero-structure (SCH) is etched with a wet chemical etch. After etching, the 200 nm thick SiN_x layer is kept on the wafer, and an additional 50 nm is deposited with PECVD. In the following lithography step, the passive waveguides are opened, while the polarization rotator areas are protected. These steps are schematically shown in Fig. 5 (a). ZEP 520A photo resist is used in this lithography with 100 kV electron beam lithography (EBL). Since the resist is only around 300 nm thick, the high topology of the etched mesa for the semiconductor optical amplifiers (SOAs) may not be fully covered by it, which is why the 200 nm thick SiNx was left on the wafer. This will protect the SOA areas, since only 50 nm SiN_x has to be etched to open the areas for n-InP etching. In Fig. 5 (b) the status of the passive waveguide (left side) and polarization rotator (right side) is shown after this opening, which is done with wet etching. For the next step another 50 nm of SiN_x is deposited on top of the previous layers. This mask is opened on the side of the vertical sidewall

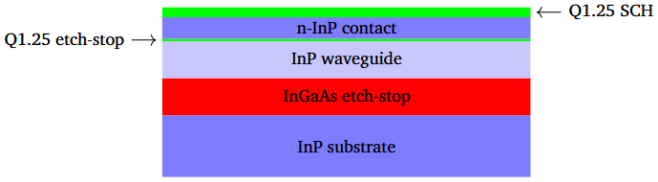

Fig. 6. Starting stack for demonstration of PR fabrication.

of the polarization rotator to create a hard mask for etching the vertical side. These steps are shown in Fig. 5 (c) & (d). An inductively coupled plasma (ICP) tool is used to etch the vertical sidewall through the n-doped InP and the waveguide layers. For the final steps another layer of 100 nm SiN_x is deposited. The areas of the rotators are opened, and the wet etch creates the triangular sections since the SiN_x protects the vertical sidewall. The final lithography and etching is graphically shown in Fig. 5 (e) & (f). After this step all SiN_x is wet chemically removed, and the fabrication of the polarization rotators is completed.

IV. Circuit Demonstrators

As a demonstration of this technology, two demonstrator circuits are presented: polarization-independent SOAs (PI-SOAs) and an integrated dual-polarization light source. Both demonstrators are briefly introduced in separate sections below, and the performance is discussed.

A. Polarization-independent SOA

For some applications it is desirable to have similar gain for the TE and TM modes from an amplifier. Since typical waveguide geometries often use quantum wells (QWs) that are optimized for providing gain to the TE mode, there is a large polarization-dependent gain (PDG). To minimize the PDG, the SOA is split in two identical halves, and a polarization rotator is integrated in between [14]. This concept is schematically shown in Fig. 7. To obtain the original input polarization state, an extra polarization rotator should be added to the circuit before or after the SOAs. In our characterization structures, this rotator was not included. For the characterization of the PI-SOAs, we define the PDG as:

$$\mathrm{PDG}\,[\mathrm{dB}] = \mathrm{abs}\left(P_{\mathrm{TE}\to\mathrm{TM}} - P_{\mathrm{TM}\to\mathrm{TE}}\right). \tag{1}$$

Since the insertion losses of the active-passive tapers are high in this particular fabrication run, the measured optical powers are relatively low. The optical spectra that are obtained for a PI-SOA with 40 mA injection current for several input wavelengths are shown in Fig. 8. Using the aforementioned formula, the PDG is obtained, which is shown in Fig. 9. At wavelengths of 1590 nm and 1600 nm, the SOA gain is low and the grating coupler loss is several decibels higher than the loss at a wavelength of 1570 nm. For the wavelengths 1570 nm and 1580 nm, a PDG of less than 3 dB for all shown injection currents is found. Note that at 1570 nm and with currents of 20 mA and 30 mA an extremely small PDG is found of only 0.24 dB. This indicates that at these conditions the

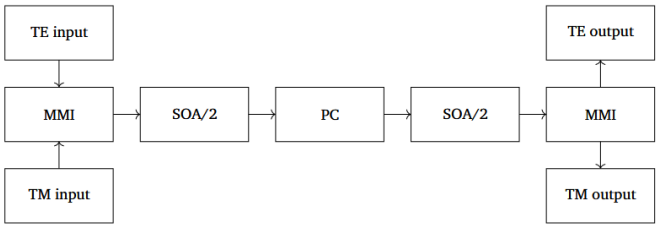

Fig. 7. Schematic of the PI-SOA concept. Schematic includes the MMIs and input/output grating couplers for TE and TM modes.

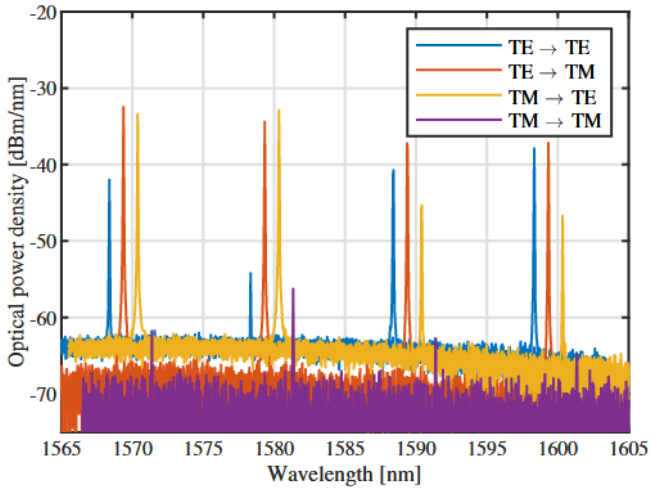

Fig. 8. Measured spectra for a PI-SOA for 40 mA injected current and several input laser wavelengths (input power is 6 dBm). Wavelengths are 1570 nm to 1600 nm in steps of 10 nm, all plotted in the same figure. Four measurements are performed at each wavelength for the four combinations of polarization. The measurements are slightly offset in wavelength for better visibility. Resolution of the optical spectrum analyzer is 0.4 nm.

polarization conversion and the identicality of the two sections are balanced. However, although it shows the potential strength of the concept, these results are somewhat accidental, since the variation in current injection between the two sections will mostly lead to thermal differences between them.

B. Dual-polarization light source

Generating light of both polarizations on the same chip can be useful for optical communication schemes or sensing applications. The dual-polarization light source consists of a Fabry-Pérot laser and a polarization rotator. The Fabry-Pérot cavity is created by a pair of photonic crystal reflectors with seven holes each. Reflectors with this number of holes have been shown to provide well above 90% reflectivity for the TE mode, for a wide wavelength range around 1550 nm [15]. The reflectivity increases with the number of holes.

When characterizing a dual polarization light source, several performance metrics are of interest, e.g. optical output power and polarization conversion efficiency (PCE). The structure that is utilized to measure these metrics is designed to couple the TE and TM polarized light to a single mode fiber separately, by using single polarization grating couplers. The

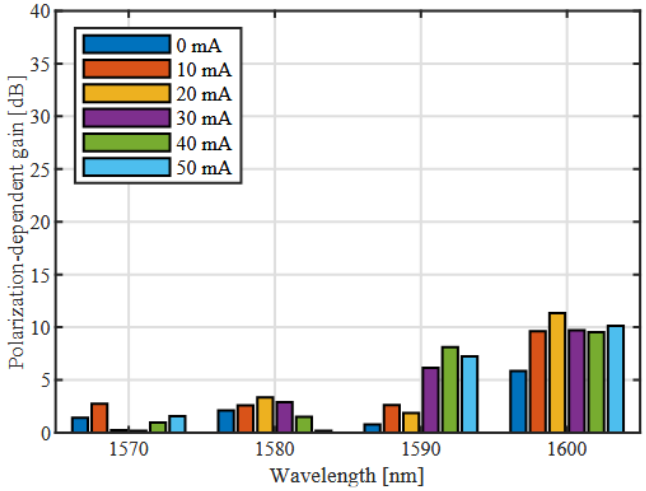

Fig. 9. Polarization-dependent gain for TE and TM inputs of a polarization-independent SOA with a single polarization rotator with section lengths of 1.6 μm and 2.5 μm.

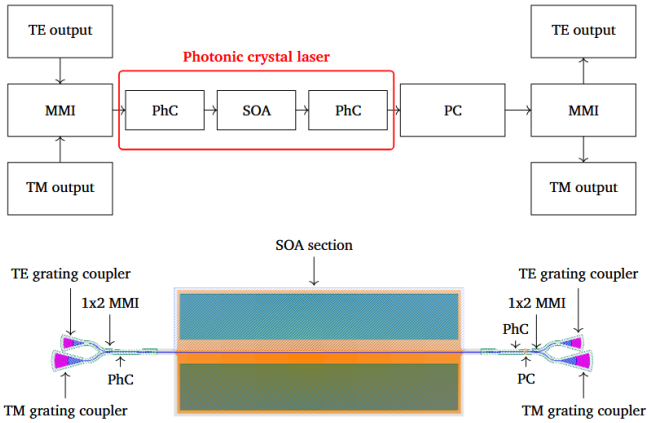

Fig. 10. Mask layout (below) and schematic (above) of a characterization structure of a laser integrated with a PC, acting as a dual-polarization light source.

schematic and mask layout of such structures are shown in Fig. 10. The characterization structure is shown in the same figure, consisting of TE and TM grating couplers for coupling light to a fiber, multimode interference couplers to split the light between the TE and TM outputs, photonic crystal reflectors with a semiconductor optical amplifier in between as a laser and a polarization rotator to convert one of the outputs to the TM mode. The laser is driven by a laser diode controller in continuous current injection mode. The Si-substrate of the IMOS chip is kept at a temperature of 15° Celsius by using a peltier element for all measurements. The output is measured with a broadband power meter, and in a separate measurement with an optical spectrum analyzer (OSA).

In Fig. 11 the measured output power at each of the grating couplers is shown: TE and TM mode on the left side (no rotator) and on the right side (with rotator). The maximum output power is around 17 μW, which is not compensated for any losses in surface grating couplers or waveguides. The

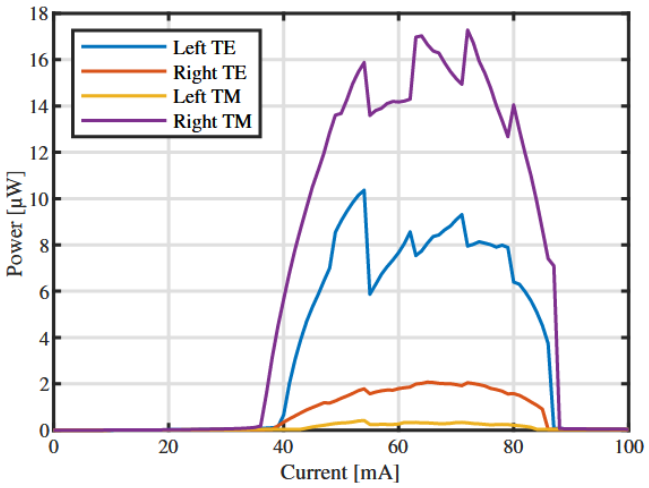

Fig. 11. Measured LI curves for a photonic crystal lasers with polarization rotator on the right output.

grating coupler loss is around 5 dB and 8 dB at a wavelength of 1550 nm for the TE and TM grating couplers, respectively. The laser wavelength is measured to be around 1585 nm, at which both grating coupler types demonstrate an insertion loss of around 15 dB.

The threshold current is around 3.5 kA/cm^2, which is higher than the threshold current on previous fabrication runs, which was around 2 kA/cm^2. This is the result of a chemical wet etch step, which etched part of the p-doped InGaAs layer of the p-contacts. Therefore, the series resistance is higher, which results in degraded performance, caused by Joule heating. The PCE (η) can be obtained from comparison of the left ($P_{\text{TE,left}}$) and the right ($P_{\text{TE,right}}$) TE-output, if the additional loss of the polarization rotator (α_{PR}) is known. Simulations show the transmission through the rotator to be 85% for both input polarizations. The two TE-outputs are then related by $P_{\text{TE,left}} = P_{\text{TE,right}} \times \alpha_{\text{PR}} \times (1 - \eta)$. From this a conversion of around 75-80% is found, slightly dependent on laser current. This value is lower than designed for and found in other devices on the same run. Most likely the reason is that the grating couplers have different, polarization-dependent losses, as is also suggested by the different power levels from both outputs.

V. Conclusion

A technology for the integration of a polarization rotator on an active-passive InP membrane platform is presented. The key fabrication steps of the integration are shown, and two demonstrator circuits are presented: a polarization-independent SOA and a dual-polarization light source. We show a PDG below 3 dB for the PI-SOAs and around 1 mW of optical power in the waveguide for both polarizations for the dual-polarization light source.

References

[1] L. M. Augustin, R. Hanfoug, J. J. G. M. van der Tol, W. J. M. de Laat, and M. K. Smit, "A Compact Integrated Polarization Splitter/Converter in InGaAsP–InP," *IEEE Photonics Technology Letters*, vol. 19, no. 17, pp. 1286–1288, Sep. 2007.

[2] M. Felicetti, J. J. G. M. van der Tol, E. J. Geluk, D. Pustakhod, M. J. Wale, and M. K. Smit, "Integrated High-Performance TE/TM Converters for Polarization Independence in Semiconductor Optical Amplifiers," *Journal of Lightwave Technology*, vol. 33, no. 17, pp. 3584–3590, Sep. 2015.

[3] D. Dai, "Ultracompact polarization diversity components for future large-scale photonic integrated circuits on silicon," in *SPIE OPTO*, J. Kubby and G. T. Reed, Eds., vol. 8629, San Francisco, California, USA, Mar. 2013, pp. 1–15.

[4] D. Dai and J. E. Bowers, "Novel concept for ultracompact polarization splitter-rotator based on silicon nanowires," *Optics Express*, vol. 19, no. 11, p. 10940, May 2011.

[5] T. Tanemura and Y. Nakano, "Compact InP Stokes-Vector Modulator and Receiver Circuits for Short-Reach Direct-Detection Optical Links," *IEICE Transactions on Electronics*, vol. E101.C, no. 7, pp. 594–601, Jul. 2018.

[6] D. Che, A. Li, X. Chen, Q. Hu, Y. Wang, and W. Shieh, "160-Gb/s Stokes Vector Direct Detection for Short Reach Optical Communication," in *Optical Fiber Communication Conference: Postdeadline Papers*. San Francisco, California: OSA, 2014, p. Th5C.7.

[7] Y. Nakano, T. Tanemura, S. Ghosh, and M. Kazi, "Stokes Vector Modulation and Detection with Monolithic InP Photonic Integrated Circuits," in *Optical Fiber Communication Conference (OFC) 2019*. San Diego, California: OSA, 2019, p. Tu2I.3.

[8] Y. Jiao, N. Nishiyama, J. J. G. M. van der Tol, J. P. van Engelen, V. Pogoretskiy, S. F. G. Reniers, A. A. Kashi, Y. Wang, V. D. Calzadilla, M. Spiegelberg, Z. Cao, K. A. Williams, T. Amemiya, and S. Arai, "InP membrane integrated photonics research," *Semiconductor Science and Technology*, vol. 36, no. 1, pp. 1–26, Jan. 2020.

[9] J. Pello, J. van der Tol, S. Keyvaninia, R. van Veldhoven, H. Ambrosius, G. Roelkens, and M. Smit, "High-efficiency ultrasmall polarization converter in InP membrane," *Optics Letters*, vol. 37, no. 17, pp. 3711–3713, Sep. 2012.

[10] S. F. G. Reniers, K. A. Williams, J. J. G. M. van der Tol, and Y. Jiao, "An Accurate Characterization Method for Integrated Polarization Converters," *IEEE Journal of Quantum Electronics*, vol. 57, no. 1, pp. 1–6, Feb. 2021.

[11] V. Pogoretskiy, "Nanophotonic membrane platform for integrated active devices and circuits," Ph.D. dissertation, Eindhoven University of Technology, Eindhoven, 2019.

[12] S. Adachi and H. Kawaguchi, "Chemical Etching Characteristics of (001) InP," *Journal of The Electrochemical Society*, vol. 128, no. 6, pp. 1342–1349, Jun. 1981.

[13] S. F. G. Reniers, V. Pogoretskiy, K. A. Williams, J. J. G. M. van der Tol, and Y. Jiao, "Towards the Integration of an Ultrashort Polarization Converter on the Active-Passive InP-Membrane-on-Silicon Platform," in *IEEE Benelux Symposium 2019*, Amsterdam, 2019, p. 5.

[14] L. M. Augustin, J. J. G. M. van der Tol, E. J. Geluk, and M. K. Smit, "Short Polarization Converter Optimized for Active–Passive Integration in InGaAsP–InP," *IEEE Photonics Technology Letters*, vol. 19, no. 20, pp. 1673–1675, Oct. 2007.

[15] S. F. G. Reniers, Y. Wang, K. A. Williams, J. J. G. M. Van Der Tol, and Y. Jiao, "Characterization of Waveguide Photonic Crystal Reflectors on Indium Phosphide Membranes," *IEEE Journal of Quantum Electronics*, vol. 55, no. 6, pp. 1–7, Dec. 2019.